Hematoporphyrin derivative photodynamic therapy induces apoptosis and suppresses the migration of human esophageal squamous cell carcinoma cells by regulating the PI3K/AKT/mTOR signaling pathway

XIN WEI*, JINLIANG NI*, LIN YUAN and XUELIANG LI

Department of Internal Medicine, First Clinical Medical College, Nanjing Medical University, Nanjing, Jiangsu 210029, P.R. China

Received August 4, 2023; Accepted November 2, 2023

DOI: 10.3892/ol.2023.14150

Abstract. Esophageal cancer is one of the most common cancer types in humans worldwide. Photodynamic therapy (PDT) is a promising therapeutic strategy for the treatment of cancer. However, its underlying mechanism needs to be studied thoroughly. The present study focused on the antitumor effect and underlying mechanism of the use of hematoporphyrin derivative (HpD)-PDT against human esophageal squamous cell carcinoma cells via regulation of the PI3K/AKT/mTOR signaling pathway. A Cell Counting Kit-8 assay was used to measure cell viability. Migration was evaluated using a wound healing assay. An annexin V-FITC/PI kit was used to determine cell apoptosis rates. Protein expression levels were analyzed via western blotting. Reverse transcription-quantitative PCR was used to detect gene expression levels. A 2',7'-dichlorodihydrofluorescein diacetate kit was chosen to evaluate intracellular reactive oxygen species levels via flow cytometry. Cell viability and migration were decreased in KYSE-150 cells after HpD-PDT treatment. Cellular apoptosis was induced after HpD-PDT treatment, and the same trend was observed for autophagy. Furthermore, the PI3K/AKT/mTOR signaling pathway was inhibited. The viability and migration of KYSE-150 cells were significantly inhibited, and apoptosis was induced more effectively following treatment with a combination of HpD-PDT and the PI3K inhibitor, a final concentration of 20 μM LY294002. In conclusion, HpD-PDT could suppress esophageal cancer cell viability, induce apoptosis and inhibit migration by downregulating the PI3K/AKT/mTOR signaling pathway. Combination of HpD-PDT with PI3K inhibitor (LY294002) could enhance the therapeutic efficacy compared with that demonstrated by HpD-PDT alone. Further studies on combination therapy are required to achieve improved clinical outcomes.

Correspondence to: Dr Xueliang Li, Department of Internal Medicine, First Clinical Medical College, Nanjing Medical University, 140 Hanzhong Road, Nanjing, Jiangsu 210029, P.R. China
E-mail: lixueliang@njmu.edu.cn

*Contributed equally

Key words: photodynamic therapy, migration, apoptosis, autophagy, PI3K

Introduction

Human esophageal cancer is one of the most prevalent cancer types worldwide. According to data published by the World Health Organization, there were ~600,000 new confirmed cases of esophageal cancer globally in 2020, accounting for 3.1% of all malignant tumors, and thus, it was ranked as the eighth most commonly occurring cancer. Esophageal cancer resulted in 540,000 deaths globally in 2020 according to data published by the International Agency for Research on Cancer, accounting for 5.5% of all deaths due to malignant tumors; thus, the mortality associated with esophageal cancer was the sixth highest. Squamous cell carcinoma is the most common type of esophageal cancer (1,2). There are a number of treatments for esophageal cancer, including endoscopic submucosal dissection for mucosal cancer, esophagectomy for locally advanced cancer and neoadjuvant chemotherapy or neoadjuvant chemoradiotherapy for terminal cancer (3).

Photodynamic therapy (PDT) has been considered to be a favorable method for the treatment of various benign or malignant diseases. There are three basic requirements for PDT: i) Photosensitizers (PSs); ii) a laser of a specific wavelength; and iii) oxygen (4). Oxygen molecules (O_2) receive the energy released from light-excited PSs, and are converted into reactive oxygen species (ROS), which results in the damage and death of neoplastic cells (5). A previous study has reported that PDT can have curative effects that cause tumor tissue necrosis, particularly in early stage tumors (6). PDT has been demonstrated to have a number of advantages during the treatment of human esophageal cancer, such as lower toxicity levels in healthy tissues (7). Furthermore, the tumor specificity is high, and the therapeutic effect of inducing cellular necrosis in skin, digestive tract, lung, vaginal and other organ tumors is marked (8). The effects of PDT are dependent on the application of PSs. PSs are specifically absorbed by tumor tissues (9). A particular wavelength of light can activate

PSs and initiate the activation processes that destroy tumor tissues (10).

Hematoporphyrin derivative (HpD) has been widely applied in PDT as a first-generation PS (5). HpD (trade name, Hiporfin) has strong photosensitivity and exhibits optimum absorption at a wavelength of 620-635 nm (11).

It is known that apoptosis is regulated and controlled via two main pathways, namely the extrinsic and intrinsic pathways. As two necessary pathways of cell apoptosis, both of them eventually lead to the induction of Caspase activation and the occurrence of apoptosis. Bcl-2 is regarded as an anti-apoptotic gene that serves a role in the intrinsic pathway (12). However, BAX serves a key role in the promotion of apoptosis (13). The ratio of the expression products of pro-apoptotic genes to anti-apoptotic genes decides whether the cell undergoes apoptosis (14). As a common result of different pathways, the Caspase protein family is activated during the apoptotic process (15). Caspase-9 initiates apoptosis, and Caspase-3 executes cell structure disassembly (16).

PI3K/Akt is a crucial signaling pathway. It is related to biological behaviors such as; cell proliferation, autophagy, cell cycle progression and apoptosis (17). Phosphorylated (p-)Akt can regulate NF-κB expression, cell proliferation and migration (18). A previous study reported that the blocking of the PI3K/Akt signaling pathway was associated with the promotion of apoptosis and suppression of tumor growth (19).

To the best of our knowledge, the connection between HpD-PDT and the PI3K/Akt signaling pathway has not been thoroughly clarified. The present study aimed to investigate the effects of HpD-PDT on the biological behavior of human esophageal squamous cell carcinoma cells and determine whether the PI3K/Akt signaling pathway is involved in the regulatory molecular mechanism of HpD-PDT based on cellular experiments.

Materials and methods

Cell culture and reagents. The KYSE-150 human esophageal squamous cell carcinoma cell line was purchased from Leibniz Institute DSMZ-German Collection of Microorganisms and Cell Cultures GmbH and short tandem repeat identification was performed. The cells were incubated in RPMI-1640 medium (Nanjing BioChannel Biotechnology Co., Ltd.). FBS (Nanjing BioChannel Biotechnology Co., Ltd.), 100 U/ml penicillin and 0.1 mg/ml streptomycin (Nanjing BioChannel Biotechnology Co., Ltd.) were added to the medium and the final FBS concentration was 10%. Cells were cultured in an incubator (Thermo Fisher Scientific, Inc.) containing 5% CO_2 at a temperature of 37˚C. All experiments involved cells in the exponential phase of growth.

The Cell Counting Kit-8 (CCK-8) was obtained from APeXBIO Technology LLC. LY294002 (cat. no. HY-10108) and 740Y-P (cat. no. HY-P0175) were obtained from MedChemExpress. The 2',7'-dichlorodihydrofluorescein diacetate (DCFH-DA) kit was purchased from Beyotime Institute of Biotechnology.

PDT protocol. HpD was purchased from Chongqing Mele Biopharmaceutical Co., Ltd. A 635-nm wavelength laser was borrowed from Guoyihuake Company. After cells became attached, the cells were divided into the following groups: Control, light, HpD and HpD-PDT. The media in the control and Light groups were replaced with fresh RPMI-1640 medium. At the same time, the media in the HpD and HpD-PDT groups were replaced with medium containing 2 mg/l HpD. After incubating cells for 4 h at 37˚C, PBS was used to wash away the residual medium. Next, fresh medium was added into all the wells. The light and HpD-PDT groups were irradiated with a 635-nm laser light at the same energy density (5 J/cm^2). The energy density was calculated using the following formula: Light energy density (J/cm^2)=power density (W/cm^2) x time (sec). All procedures were performed in the darkroom and plates were covered with foil.

Detection of intracellular HpD. HpD exhibits red fluorescence when exposed to a 390-450-nm light source, rendering it well-suited for early clinical tumor fluorescence diagnosis (20). Therefore, by utilizing a fluorescence microscope within the appropriate wavelength range, it was possible to directly visualize the cellular uptake of HpD. Cells (5x10^5 cells/ml) were seeded into 6-well plates and incubated with 2 mg/l HpD for different durations (1, 2, 4 and 8 h) at 37˚C. The intracellular uptake of HpD was assessed by fluorescence microscopy (Nikon ECLIPSE Ti; Nikon Corporation).

Cell viability. KYSE-150 cells (1x10^5 cells/ml) were added into 96-well plates and incubated in RPMI-1640 medium. The old media were substituted with fresh media containing HpD at various concentrations, ranging from 0 to 8 mg/l, the next day. After incubating the cells for 4 h at 37˚C in the dark, PBS was used to wash away HpD that had not been absorbed by cells. The plates were irradiated under 635-nm light with different energy levels (0, 2.5, 5 and 7.5 J/cm^2). Subsequently, cells were cultured in a dark room. After 24 h, the culture medium was substituted with 100 μl fresh medium containing CCK-8 reagent. After incubating cells for 2 h in the dark, the optical densities (ODs) were measured at 450 nm using a microplate reader (Thermo Fisher Scientific, Inc.). The following formula was used to estimate cell viability: Cell viability (%)=[(mean OD of experiment group-mean OD of the blank group)/(mean OD of control group-mean OD of blank group)] x100. The wells of the control group only contained fresh RPMI-1640 medium and CCK-8 solution.

ROS measurement. The DCFH-DA kit was used to measure ROS levels. KYSE-150 cells were seeded in 6-well plates (1x10^5 cells/ml) and incubated for 12 h in the cell culture incubator at a temperature of 37˚C. The culture medium for the HpD and HpD-PDT groups was replaced with medium containing 2 mg/l HpD. The control and Light groups were maintained in serum-free medium. After incubating all cells in the dark for 4 h in a 37˚C incubator, the HpD-PDT group was subjected to light exposure (5 J/cm^2). The medium was completely replaced with medium containing DCFH-DA diluted to a concentration of 10 μM. After 30 min, KYSE-150 cells were rinsed with PBS at least three times. All cells were trypsinized and collected. A flow cytometer (Cytoflex S; Beckman Coulter, Inc.) was used to detect the fluorescence intensity level. The data was analyzed using CytExpert

(version 2.4; Beckman Coulter) and GraphPad Prism software (version 8.3.0; Dotmatics).

Wound healing assay. KYSE-150 cells were cultured in 6-well plates. When the cells were almost 100% confluent, the HpD and HpD-PDT groups were incubated with RPMI-1640 medium containing HpD (1 mg/l) for 4 h. Several sterile 10-μl pipet tips were used to create scratches. Residual floating cells were washed away carefully with PBS. The cell culture medium was substituted with serum-free medium. The light and HpD-PDT groups were subjected to the irradiation process immediately (2.5 J/cm^2). Cells in the control and HpD groups continued to be incubated in the dark at 37˚C in the incubator. All images were captured immediately or 12 h later under a light microscope. ImageJ was used to convert the original images to grayscale images and to measure the area of the scratches. The scratch migration rate was calculated using the following formula: Migration rate=(Scratch area at 0 h-scratch area at 12 h)/scratch area at 0 h.

Hoechst 33342 staining. Cells were cultured overnight in 12-well plates (5x10^5 cells/ml). After subjecting them to different treatments (control, HpD, light and HpD-PDT), cells were continuously cultured for 24 h. Subsequently, KYSE-150 cells were incubated for 30 min in a dark room with Hoechst 33342 staining solution (Beyotime Institute of Biotechnology) at room temperature. Pre-cooled PBS was used to wash off the residual solution at least three times. A Thunder Imager fluorescence microscope (Leica Microsystems GmbH) was used to capture images.

Cell apoptosis. The cell apoptosis rate was measured using an Annexin V-FITC/PI Kit (Vazyme Biotech Co., Ltd.). KYSE-150 cells were grown in 6-well plates (2x10^5 cells per well). After subjecting the cells to different treatments (control, HpD, light and HpD-PDT), the HpD and HpD-PDT group were incubated with fresh medium containing 2 mg/l HpD for 4 h. Subsequently, the Light group and HpD-PDT group received laser irradiation (5 J/cm^2). Cells were incubated for 24 h in a 5% CO_2 incubator at 37˚C. After cells were trypsinized, washed and centrifuged at 300 x g for 5 min at 4˚C to remove the supernatant, the cell precipitate in each tube was resuspended using 100 μl binding buffer containing an appropriate volume of FITC and PI. Subsequently, cells were placed in the dark for 20 min. Finally, 400 μl binding buffer was added to the cell suspension. FITC-positive cells were detected using a flow cytometer (Cytoflex S; Beckman Coulter). The cell apoptosis rate was calculated by determining the proportion of early apoptotic cells (FITC-positive/PI-negative) and late apoptotic cells (FITC-positive/PI-positive) among all cells. The data were analyzed using CytExpert (version 2.4; Beckman Coulter) and GraphPad Prism software (version 8.3.0; Dotmatics).

Reverse transcription-quantitative PCR (RT-qPCR) analysis. After cell grouping (control, HpD, light and HpD-PDT), the HpD group and HpD-PDT group were incubated with fresh medium containing 2 mg/l HpD for 4 h. The Light group and HpD-PDT group received laser irradiation (5 J/cm^2). All groups of cells were incubated in the dark at 37˚C in a cell culture incubator for 24 h. RNAiso Plus (Takara Bio, Inc.) was used to extract RNA at 24 h post-HpD-PDT. Subsequently, 75% ethanol was used to purify the extracted RNA. An ultraviolet spectrophotometer was used to measure the concentration of RNA. Reverse transcription was performed to synthesize cDNA. A HiScript II Q RT SuperMix for qPCR kit (Vazyme Biotech Co., Ltd.) was used for reverse transcription. This process was conducted under the following reaction conditions: 50˚C for 15 min and 85˚C for 5 sec. SYBR Green Mix (Vazyme Biotech Co., Ltd.) was used to perform qPCR using StepOne Plus (Applied Biosystems; Thermo Fisher Scientific, Inc.). The program was set as follows: i) Holding stage, 95˚C for 30 sec; ii) cycling stage (40 cycles), 95˚C for 10 sec and 60˚C for 30 sec; and iii) melting curve stage, 95˚C for 15 sec, 60˚C for 1 min and 95˚C for 15 sec. The $2^{-\Delta\Delta Cq}$ method was used (21). GAPDH was chosen as the reference gene. TsingKe Biological Technology synthesized the primers. All primer sequences are listed in Table I.

Table I. Primer sequences for target genes.

Gene name	Primer sequences (5'-3')
GAPDH	F: CACCATCTTCCAGGAGCGAG
	R: GATGGCATGGACTGTGGTCA
Bcl-2	F: TTCTTTGAGTTCGGTGGGGTC
	R: TGCATATTTGTTTGGGGCAGG
BAX	F: TCCACCAAGAAGCTGAGCGAG
	R: GTCCAGCCCATGATGGTTCT
Caspase 3	F: CATGGAAGCGAATCAATGGACT
	R: CTGTACCAGACCGAGATGTCA
Caspase 7	F: AGTGACAGGTATGGGCGTTC
	R: CGGCATTTGTATGGTCCTCTT'
PTEN	F: TTTGAAGACCATAACCCACCAC
	R: ATTACACCAGTTCGTCCCTTTC

F, forward; R, reverse.

Western blotting. RIPA lysis buffer (Beyotime Institute of Biotechnology) containing PMSF and phosphatase inhibitors purchased from Bimake.com was used to lyse KYSE-150 cells. A BCA kit (Beyotime Institute of Biotechnology) was used to quantify protein concentrations. SDS-PAGE was performed to isolate proteins with 12.5% gels. The mass of protein loaded per lane was 30 μg. Target proteins were transferred to PVDF membranes (Roche Diagnostics GmbH). Bovine serum albumin powder (Biosharp) was dissolved in tris-buffered saline with 0.1% Tween 20 (TBST) to block membranes and membranes were agitated for 1.5 h at room temperature. The concentration of bovine serum albumin solution was 5%. The membranes were incubated with primary antibodies overnight at 4˚C. TBST was used to wash the membranes three times the next day. Next, the membranes were incubated with the secondary antibody for 2 h at 4˚C. A NcmECL Ultra kit (New Cell and Molecular Biotech Co., Ltd.) was used to identify the target protein bands. All images were processed using ImageJ (version 1.53 C; National Institutes of Health). Phospho-PI3K (rabbit anti-human; cat. no. 4228; dilution, 1:1,000), mTOR

(rabbit anti-human; cat. no. 2983; dilution, 1:2,000) and phospho-mTOR (Ser2448) (rabbit anti-human; cat. no. 5536; dilution, 1:1,000) primary antibodies were provided by Cell Signaling Technology, Inc. The following antibodies were supplied by Proteintech Group, Inc.: Bcl-2 (mouse anti-human; cat. no. 60178-1-Ig; dilution, 1:2,000), BAX (mouse anti-human; cat. no. 60267-1-Ig; dilution, 1:5,000), Caspase-3 (mouse anti-human; cat. no. 66470-2-Ig; dilution, 1:1,000), LC3 (rabbit anti-human; cat. no. 14600-1-AP; dilution, 1:2,000), p62 (mouse anti-human; cat. no. 18420-1-AP; dilution, 1:5,000), GAPDH (mouse anti-human; cat. no. 60004-1-Ig; dilution, 1:50,000), β-actin (mouse anti-human; cat. no. 66009-1-Ig; dilution, 1:20,000), PI3Kinase p85 (mouse anti-human; cat. no. 60225-1-Ig; dilution, 1:5,000), AKT (mouse anti-human; cat. no. 60203-2-Ig; dilution, 1:5,000), phospho-AKT Ser473 (mouse anti-human; cat. no. 66444-1-Ig; dilution, 1:5,000), HRP-conjugated Affinipure Goat Anti-Rabbit (cat. no. SA00001-2; dilution, 1:2,000), HRP-conjugated Affinipure Goat Anti-Mouse (cat. no. SA00001-1; dilution, 1:2,000), E-cadherin (mouse anti-human; cat. no. 20874-1-AP; dilution, 1:20,000) and N-cadherin (mouse anti-human; 22018-1-AP; dilution, 1:2,000).

Combined experiments. For the combined experiments, cells ($1x10^5$cells/ml) were added into 96- and 6-well plates. In the experimental group, cells were incubated in serum-free medium containing 740Y-P or LY294002 at a range of concentrations (10, 20, 30 and 40 μM) at 37˚C, whereas the control group was treated with RPMI 1640 medium. After 12 h, experimental group cells were incubated in serum-free medium containing 2 mg/l HpD. After 4 h, the cells were irradiated with the laser in the PDT-alone group and combined group.

Statistical analysis. All experiments were independently repeated three times. Data analysis and mapping were performed using GraphPad Prism software (version 8.3.0; Dotmatics). Data are presented as the mean ± SD and were analyzed by one-way ANOVA, with Tukey's method was used for post-hoc analysis. $P<0.05$ was considered to indicate a statistically significant difference.

Results

HpD-PDT suppresses KYSE-150 cell viability. The cellular uptake of HpD increased over time. After a 4-h incubation, cells had absorbed a substantial amount of HpD. After an 8-h incubation, the cellular uptake of HpD was similar to that after 4 h of incubation (Fig. 1A). Cells were incubated with HpD in the dark for 4 h in the subsequent experiments, allowing the PS sufficient time to enter the cells, while minimizing changes in the microenvironment of the cell culture medium (22). To investigate the most appropriate laser energy density and concentration of HpD, KYSE-150 cells were subjected to HpD and energy at different concentration gradients. When cells were in a completely dark environment (0 J/cm^2), increasing concentrations of HpD had no cytotoxicity. The cell viability after HpD-PDT treatment was decreased in a dose-dependent manner. The efficacy was dependent on the combination of the HpD concentration and energy density (Fig. 1B). Cell viability plateaued when the HpD concentration was increased to 6 mg/l. When the energy density was 5 J/cm^2 and the HpD concentration was 2 mg/l, the mean survival rate of KYSE-150 cells was 52.77%. To avoid interference from excessively high or low HpD concentrations and light intensities on the experimental results, parameters with moderate light intensity and HpD concentration were chose. Finally, a concentration of 5 J/cm^2 in combination with 2 mg/l HpD was selected for all subsequent experiments except for the wound healing assay.

ROS levels are significantly increased after HpD-PDT. The intracellular ROS levels were quantified after HpD-PDT. Analysis based on flow cytometry demonstrated that the relative fluorescence intensities of the control, light, HpD and HpD-PDT groups were 5.99±0.13, 5.49±0.27, 6.05±0.41 and 9.81±0.39, respectively. The ROS level of the control group was notably lower than that of the HpD-PDT group (Fig. 1C and D). However, the differences in ROS levels among the control, light and HpD groups were not statistically significant ($P=0.1099$). The present study also evaluated the production of ROS following PDT treatment (light energy density, 5 J/cm^2) at various concentrations of HpD. There was no significant difference in ROS production between the concentrations of 2 and 4 mg/l. When the HpD concentration was increased to 6 mg/l, there was a significant increase in ROS production compared with the 4 mg/l group (Fig. 1E and F).

HpD-PDT suppresses KYSE-150 cell migration. Based on the results of the cell viability assay, low-dose light (2.5 J/cm^2) in combination with 1 mg/l HpD was selected for the wound healing assay, to avoid the effects of cell death on cell migration. After 12 h, the scratch healing rates of the control, light, HpD and HpD-PDT groups were 73.77±0.09, 62.08±0.06, 67.45±0.04 and 18.89±0.03%, respectively. These results suggested that HpD-PDT significantly suppressed the migration of KYSE-150 cells (Fig. 2A and B). It is well-known that epithelial-mesenchymal transition (EMT) serves a key role in cell migration. N-cadherin is a mesenchymal marker, while E-cadherin is an epithelial marker. A marker event of EMT is the downregulation of E-cadherin and the increased expression of N-cadherin, also known as the 'cadherin switch'. It results in lost epithelial cell integrity, decreased epithelial intercellular adhesion and enhanced cell migration (23,24). To understand the underlying mechanism of PDT in the inhibition of cell migration, western blotting was performed to assess E-cadherin and N-cadherin expression. E-cadherin protein expression was upregulated after HpD-PDT treatment. By contrast, N-cadherin expression was decreased significantly compared with that of the control group. These results indicated that HpD-PDT inhibited the EMT process, which in turn inhibited cell migration (Fig. 2C-E).

HpD-PDT induces cell autophagy. To understand the relationship between cell autophagy and HpD-PDT treatment, the expression levels of autophagy-associated proteins were assessed. LC3 has been studied most often as a distinctive autophagy marker. LC3 I can be transformed to LC3 II during autophagy, indicating the level of autophagy activity. p62 is considered a vital protein during autophagy (25). p62 can interact with LC3 on the isolation membrane through the

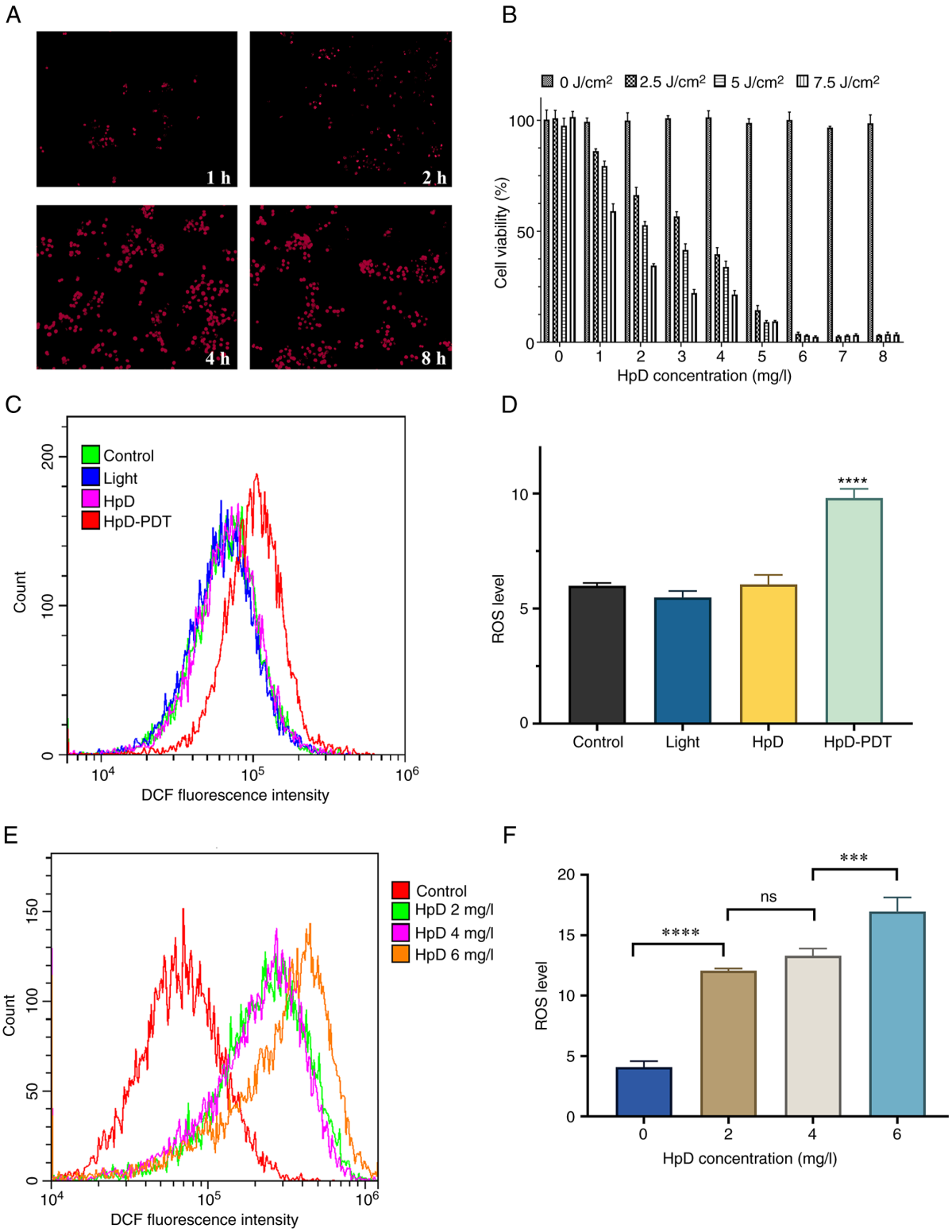

Figure 1. Cytotoxicity of HpD-PDT in KYSE-150 cells. (A) Cellular uptake of HpD at different incubation times was determined using fluorescence microscopy (magnification, x200). (B) Cytotoxicity of HpD-PDT was examined using a Cell Counting Kit-8 assay. The cells were incubated with HpD in the dark for 4 h and then underwent 635-nm laser irradiation, followed by a CCK-8 assay 24 h later. The cell viability was decreased in a dose-dependent manner. (C) Detection of the ROS levels via 2',7'-dichlorodihydrofluorescein diacetate staining. (D) Intracellular ROS was quantified (mean ± SD; n=3; ****P<0.0001 vs. control group). All data were obtained from three independent replicate samples. The statistical test used was ANOVA. (E) Flow cytometry was used to detect intracellular ROS levels in cells incubated with different concentrations of HpD and subjected to PDT treatment. (F) When the HpD concentration was 6 mg/l, the highest ROS production was observed after cellular PDT treatment. ***P<0.001 and ****P<0.0001. HpD, hematoporphyrin derivative; ns, not significant; PDT, photodynamic therapy; ROS, reactive oxygen species.

LC3-interacting area. During the process of autophagosome formation in cells, p62 is incorporated into the autophagosome and is subsequently degraded (26). Autophagy activation is usually accompanied by p62 degradation (27). LC3 II protein

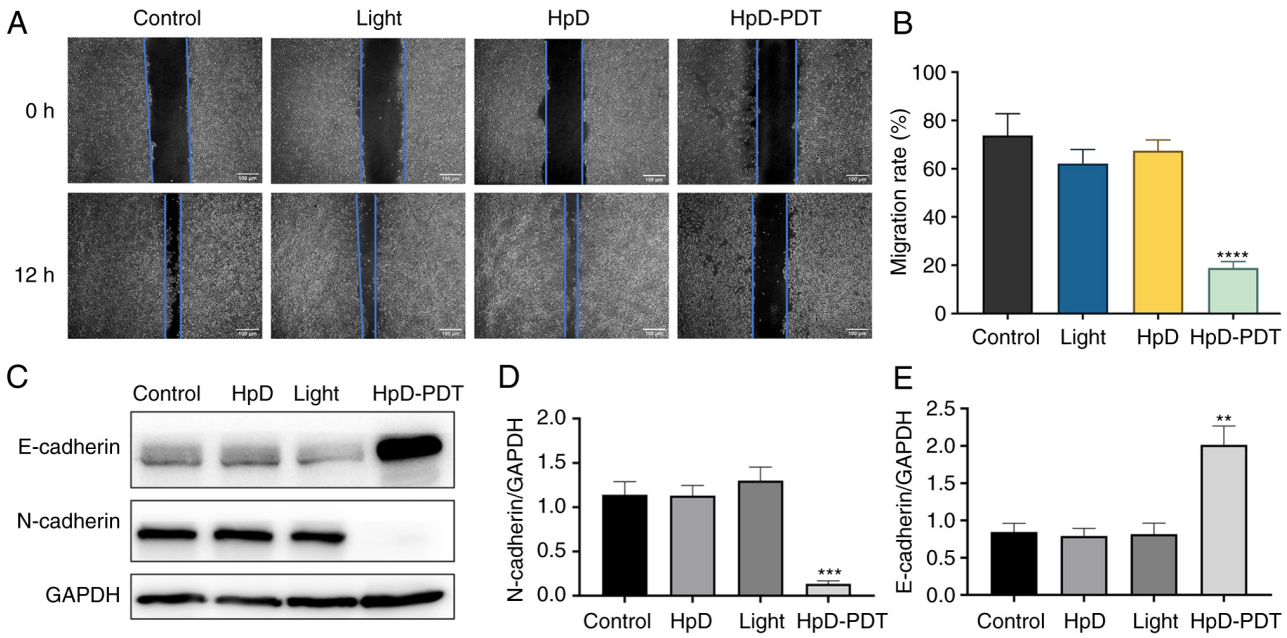

Figure 2. Effects of HpD-PDT on cell migration and epithelial-mesenchymal transition. (A) A wound healing assay was used to detect the effect of HpD-PDT on migration. Scale bar, 100 μm. The original images were converted to grayscale images using ImageJ. (B) HpD-PDT significantly inhibited the migration of KYSE-150 cells (mean ± SD; n=3; ****P<0.0001 vs. control group). (C) The protein expression of E-cadherin and N-cadherin was detected by western blotting. (D) N-cadherin expression was significantly decreased (mean ± SD; n=3; ***P<0.001 vs. control group). (E) E-cadherin expression was upregulated after HpD-PDT treatment (mean ± SD; n=3; **P<0.01 vs. control group). HpD, ematoporphyrin derivative; PDT, photodynamic therapy.

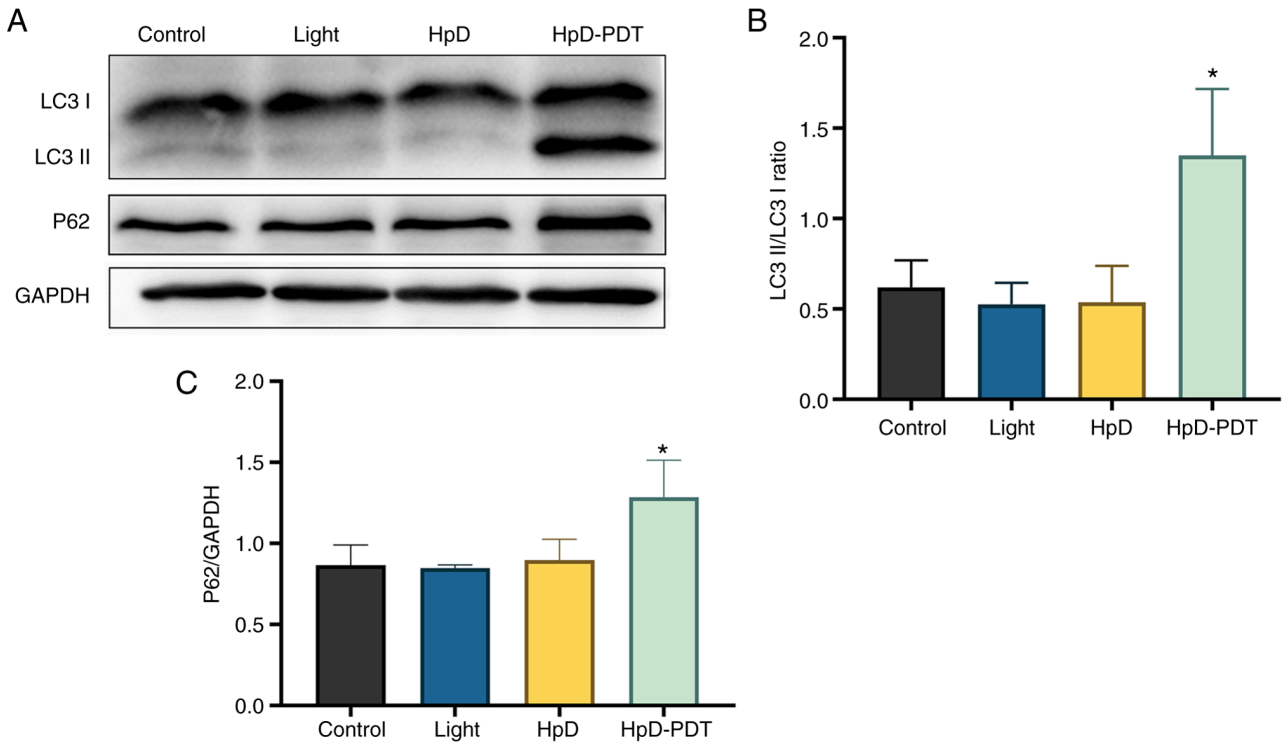

Figure 3. HpD-PDT induces autophagy in KYSE-150 cells. (A) LC3 and p62 protein expression was detected by western blotting. (B) The ratio of LC3 II to LC3 I was increased in the HpD-PDT group (mean ± SD; n=3; *P<0.05 vs. control group). (C) p62 expression was increased in the HpD-PDT group 24 h after irradiation (mean ± SD; n=3; *P<0.05 vs. control group). All bands were normalized to those of GAPDH. HpD, ematoporphyrin derivative; PDT, photodynamic therapy.

levels were increased at 24 h after irradiation in the HpD-PDT group, causing the ratio of LC3 II to LC3 I to be significantly increased compared with those in the control (Fig. 3A and B). However, the protein expression levels of p62 were also significantly upregulated after HpD-PDT treatment compared with those in the control (Fig. 3C). We hypothesized that although

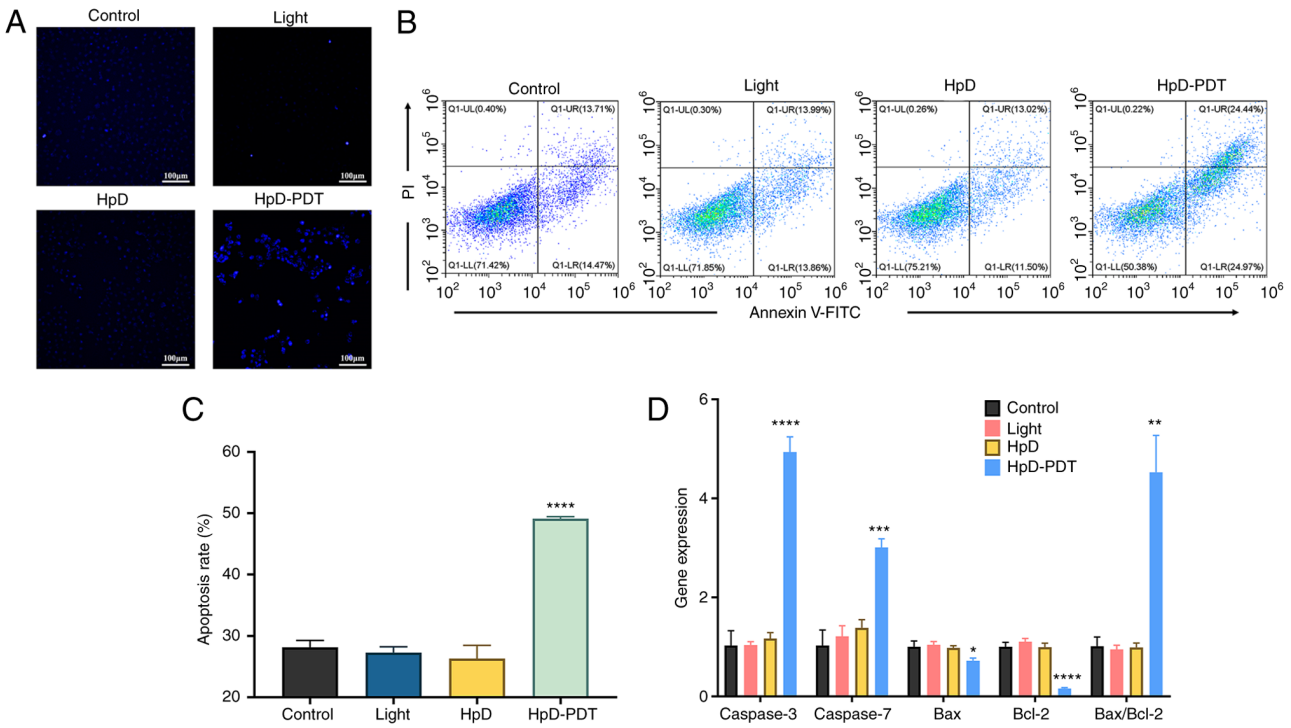

Figure 4. HpD-PDT induces apoptosis in KYSE-150 cells. (A) Cells were stained with Hoechst 33342 and images were captured using a fluorescence microscope (scale bar, 100 μm). (B) Cell apoptosis rates were determined using flow cytometry with an annexin V-FITC/PI kit. (C) The apoptosis rates of the control, light, HpD and HpD-PDT groups were 28.15±1.12, 27.28±0.95, 26.31±2.16 and 49.13±0.32%, respectively. The percentage of apoptotic cells was significantly increased after HpD-PDT treatment (mean ± SD; n=3; ****P<0.001 vs. control group). (D) Expression levels of apoptosis-related genes were detected by reverse transcription-quantitative PCR 24 h after laser irradiation (mean ± SD; n=3; *P<0.05, **P<0.01, ***P<0.001 and ****P<0.0001 vs. control group). HpD, ematoporphyrin derivative; PDT, photodynamic therapy.

HpD-PDT could induce autophagy, the increased p62 protein levels indicated a decrease in autophagic flux.

HpD-PDT-induced apoptosis in KYSE-150 cells. To visualize apoptotic cells, a Hoechst 33342 staining assay was performed. The nuclei of apoptotic cells exhibited bright blue fluorescence. Only a few apoptotic cells could be found among the control, light and HpD groups. By contrast, numerous apoptotic cells were observed in the HpD-PDT group (Fig. 4A). Subsequently, cell apoptosis levels were examined via flow cytometry. Annexin V-FITC/PI staining was performed at 24 h after PDT. Both early and late apoptotic cells manifested as FITC-positive cells. The percentages of apoptotic cells were determined (Fig. 4B and C). In the HpD-PDT group, the percentage of apoptotic cells was markedly higher than that in other groups. To further investigate the relationship between apoptosis and HpD-PDT treatment, RT-qPCR was used to evaluate the expression of specific genes related to apoptosis. The results of RT-qPCR (Fig. 4D) demonstrated that Bcl-2 expression was significantly downregulated after PDT compared with that in the control; thus, the ratio of BAX to Bcl-2 was significantly increased. Additionally, HpD-PDT significantly upregulated Caspase-3 gene expression compared with the control (Fig. 4D). The protein expression levels of cleaved Caspase-3, which is vital for converting normal cells into apoptotic cells (28), were significantly increased following HpD-PDT compared with the control (Fig. 5A). The expression levels of Bcl-2 were also notably decreased in HpD-PDT-treated cells compared with control. The expression levels of BAX did not show significant intergroup differences. These results indicated that HpD-PDT induced apoptosis in KYSE-150 cells.

HpD-PDT reduces phosphorylation levels in the PI3K/Akt/mTOR signaling pathway. KYSE-150 cells were collected at 24 h after HpD-PDT. Western blotting was subsequently performed to determine changes in the PI3K/Akt/mTOR signaling pathway after HpD-PDT treatment. The results demonstrated that the ratios of p-PI3K/PI3K and p-mTOR/mTOR were significantly decreased after HpD-PDT (Fig. 5A). The PI3K signaling pathway can be negatively regulated by PTEN (29). By decreasing the phosphatidylinositol-3, 4, 5-phosphate levels inside the cell, PTEN can serve a physiological role to inhibit the activation of downstream proteins of the PI3K signaling pathway (30). Therefore, PTEN expression could be used to indirectly detect the activity of the PI3K signaling pathway. PTEN expression examined by qPCR was significantly increased after HpD-PDT compared with the control (Fig. 5B). These findings demonstrated that HpD-PDT inhibited the activation of the PI3K signaling pathway. After pre-treating the cells with the PI3K activator 740Y-P for 12 h, cell viability was assessed using a CCK-8 assay. As the concentration of 740Y-P increased, it did not enhance cell viability following HpD-PDT treatment (Fig. 5C). An artificial inhibitor of PI3K (LY294002) was used to determine the relationship between the PI3K/Akt/mTOR signaling pathway and HpD-PDT. LY294002, a well-known PI3K signaling pathway inhibitor, could simultaneously inhibit the activity

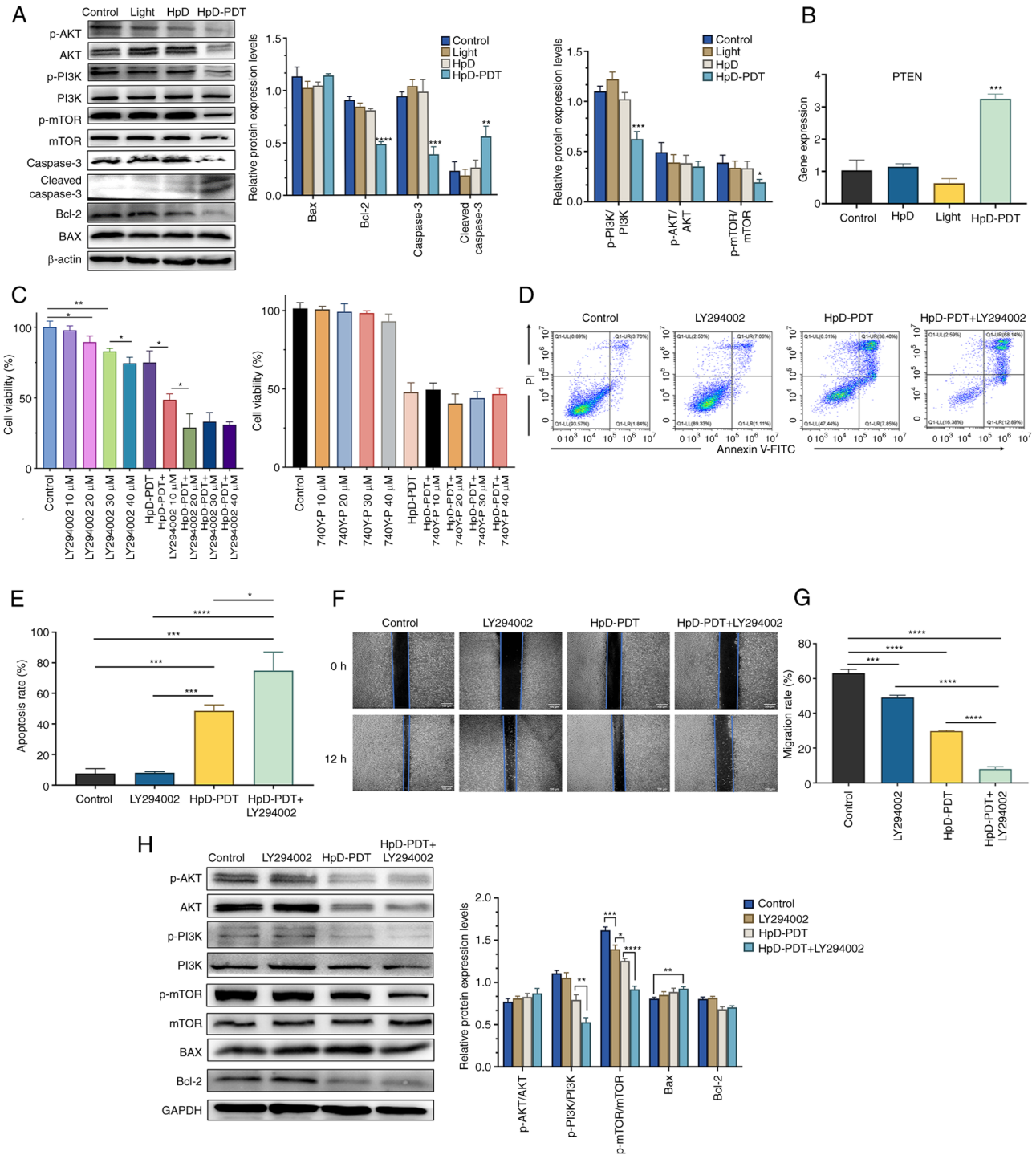

Figure 5. Role of the PI3K/AKT/mTOR signaling pathway in HpD-PDT treatment. (A) Phosphorylation levels of PI3K, AKT and mTOR were detected by western blotting. The expression levels of apoptosis-related proteins were also detected (mean ± SD; n=3; *P<0.05, **P<0.01, ***P<0.001 and ****P<0.0001 vs. control group). (B) PTEN expression was measured by reverse transcription-quantitative PCR 24 h after laser irradiation (mean ± SD; n=3; ***P<0.001 vs. control group). (C) Effect of combined treatment on cell viability was measured using a Cell Counting Kit-8 assay 24 h after laser irradiation (*P<0.05 and **P<0.01). (D) Flow cytometry analysis of apoptosis in KYSE-150 cells was performed based on Annexin V/PI staining. (E) Cell apoptosis was higher in the combination group than in the HpD-PDT alone group (mean ± SD; n=3; LY294002 + HpD-PDT group vs. HpD-PDT group; *P<0.05, ***P<0.001 and ****P<0.0001). (F) Representative images of cellular migration after different treatments (scale bar, 100 μm). The original images were converted to grayscale images using ImageJ. (G) Combination of HpD-PDT with LY294002 could enhance the efficiency of inhibition of cell migration compared with that observed for HpD-PDT alone (mean ± SD; n=3; ***P<0.001; ****P<0.0001). (H) Phosphorylation levels of PI3K, AKT and mTOR in the LY294002 + HpD-PDT group were detected by western blotting. The protein expression levels of BAX and Bcl-2 were also detected (mean ± SD; n=3; *P<0.05, **P<0.01, ***P<0.001 and ****P<0.0001). HpD, ematoporphyrin derivative; p-, phosphorylated; PDT, photodynamic therapy.

of PI3Kα, PI3Kδ and PI3Kβ (31). The CCK-8 assay was used to verify whether LY294002 exerted notable levels of cytotoxicity. Cells were incubated with LY294002 for 12 h before irradiation in the LY294002 only group (LY294002 group) and combination group (LY294002 + HpD-PDT group). The results of the CCK-8 assay demonstrated no

significant difference at a 10 μM LY294002 concentration in the LY294002 group. However, the cell viability gradually decreased as the LY294002 concentration increased. If the LY294002 concentration reached 40 μM, the degree of the inhibition effect was almost similar to that observed with HpD-PDT. In addition, cell viability was significantly decreased in the LY294002 10 μM + HpD-PDT group compared with the HpD-PDT alone group (Fig. 5C). When the LY294002 concentration increased to 20 μM in the combination group, cell viability was further reduced. No statistical differences were observed among the LY294002 20 μM + HpD-PDT, LY294002 30 μM + HpD-PDT and LY294002 40 μM + HpD-PDT groups. Continuing to increase the concentration of LY294002 did not result in a better enhancement of PDT efficacy. Finally, 20 μM LY294002 was selected for the subsequent experiment. Flow cytometry was performed again to assess the apoptosis rate. In the combination group, the apoptosis rate was markedly higher than that in the LY294002 only and HpD-PDT only groups (Fig. 5D and E). The present findings suggested that the combination of HpD-PDT with LY294002 enhanced the pro-apoptotic effects of HpD-PDT. To further explore their combinatorial effects on KYSE-150 cell migration, a wound healing assay was performed. In the combined treatment group, the migration of cells was significantly suppressed compared with that observed in the HpD-PDT alone or LY294002 alone groups (Fig. 5F and G). Furthermore, protein expression levels in the combined treatment group and the HpD-PDT-alone group were assessed using western blotting. The ratios of p-PI3K/PI3K and p-mTOR/mTOR in the LY294002 + HpD-PDT group were significantly decreased compared with those in the HpD-PDT alone group. By contrast, the ratio of p-AKT/AKT did not exhibit significant inter-group differences. The expression levels of Bcl-2 were also markedly decreased in both the HpD-PDT alone group and the LY294002 + HpD-PDT group. However, there were no significant differences between the two groups (Fig. 5H).

Discussion

PDT has been regarded as an accepted non-invasive PS application-based therapy that can be activated by light (10). Compared with other treatments, such as surgery, radiotherapy, chemotherapy or a combination of these therapies used for esophageal squamous cell carcinoma, PDT has certain advantages, including high tumor specificity, minimal side effects and relatively minor tumor resistance (32). Certain scholars have proposed that the tumor microenvironment could potentially lead to PDT resistance. Intervening in the tumor microenvironment may reduce this resistance (33,34). PDT has been recommended and applied for the treatment of malignant tumor (35). Nevertheless, to the best of our knowledge, its underlying mechanism has not been studied thoroughly.

A positive association was observed between ROS production and the HpD concentration in PDT. With the increase in HpD concentration, there was a simultaneous increase in ROS production, while the maximum inhibition of cell viability was achieved. At an HpD concentration of 6 mg/l, both the inhibition of cell viability and ROS production reached significantly high levels compared with the control. This implied that increasing ROS production was crucial for the efficacy of HpD-PDT.

The present study revealed that HpD-PDT had the ability to reduce KYSE-150 cell viability, in a HpD concentration and laser energy density-dependent manner, and HpD-PDT could inhibit the migration of esophageal squamous cells by suppressing the EMT process. Tumor cells exhibiting a strong ability to invade usually exhibit an increased degree of malignancy (36). The extracellular matrix (ECM) is critical for processes such as migration and invasion (18). It has been reported that MMPs could affect ECM degradation, which could affect the metastasis and invasion of tumor cells (37). MMP-2 and MMP-9, two representative proteins, are closely related to tumor metastasis (38). The PI3K/Akt signaling pathway is also closely linked with the regulation of MMP expression (39). p-Akt could trigger the regulation of MMP-2 and MMP-9 (40,41). Further research is required to determine whether PDT can indirectly regulate the MMP protein family and influence cell invasion through the PI3K/AKT signaling pathway.

Autophagy has been considered a mechanism by which tumor cells respond to stress and starvation during changes in the external environment (42). This cellular self-digestion could remove damaged proteins or impaired organelles to keep the cells alive; however, it could also cause autophagic death of tumor cells (27). Therefore, autophagy has a dual regulatory ability because it can lead to cell survival or death based on different external stimulus conditions (43). A number of tumor therapies induce autophagic death by adjusting cell signaling pathways, and can indirectly induce autophagy by exerting cytotoxic effects (42). However, to the best of our knowledge, the efficacy of autophagy induction during the cancer treatment process remains unclear. The PI3K/AKT/mTOR signaling pathway has been studied extensively to investigate and determine its role in autophagy regulation (44-46). The PI3K pathway has been demonstrated to act as a crucial mechanism for cellular autophagy that helps deal with changes in ROS levels. The downstream protein Akt participates in this process by activating the mTOR complex (mTORC)1 (44). Furthermore, Akt could inhibit autophagy-related gene expression. Under low ROS level conditions, mTORC1 and mTORC2 could suppress cell autophagy (44). Under high ROS level conditions, mTORC2 could accelerate cellular aging via the promotion of autophagy (44). As expected, LC3 II expression was markedly increased after HpD-PDT, which in turn resulted in the ratio of LC3 II to LC3 I increasing significantly, indicating the occurrence of autophagy. p62/sequestosome 1 expression increased after HpD-PDT treatment. p62 is involved in the autophagy process as a substrate. It is degraded when the autophagosome is formed. Alternatively, it can be accumulated due to impairments in autophagic flux (42). We hypothesized that HpD-PDT may block the autophagic flux, causing p62 accumulation and ultimately resulting in cell death (47). Briefly, HpD-PDT initiated autophagy in KYSE-150 cells, followed by the blockade of autophagic flux.

Apoptosis is considered to be a programmed cell death process. This process is related to the activation of the cysteine protease family (48). As aforementioned, apoptosis is regulated and controlled via two main pathways. Both

pathways eventually lead to Caspase activation. However, the final apoptotic process is initiated with the cleavage of Caspase-3, which causes DNA to be broken into fragments and the cytoskeleton to be degraded. Finally, those fragments are swallowed by phagocytic cells (49). The present study revealed that HpD-PDT triggered Caspase-dependent apoptosis in KYSE-150 cells. The levels of cleaved Caspase-3 were significantly increased following HpD-PDT. In addition, the protein expression levels of Bcl-2, which is known as an anti-apoptotic gene, were downregulated after HpD-PDT treatment. However, the protein expression levels of BAX did not exhibit significant intergroup differences. These results indicated that the balance between pro-apoptotic and anti-apoptotic effects was broken. Additionally, the increase in the ROS levels may be the factor driving these changes.

The present study demonstrated that the ratios of p-PI3K/PI3K and p-mTOR/mTOR were significantly decreased following HpD-PDT. It is evident that the PI3K/AKT/mTOR signaling pathway plays a significant role in the process through which PDT exerts the aforementioned therapeutic effects.

CCK-8 assays were performed using cells pre-treated with 740Y-P, and it was observed that 740Y-P was unable to counteract the inhibitory effect of HpD-PDT on cell viability. We hypothesized that PDT may encompass certain mechanisms for tumor cell eradication, with the modulation of the PI3K/AKT/mTOR signaling pathway representing merely one facet of the multifaceted interplay. In situations where the PI3K/AKT/mTOR signaling pathway cannot be inhibited, PDT has the potential to induce cell death via alternative mechanisms, such as pyroptosis and ferroptosis (50-54).

LY294002, a broad-spectrum PI3K inhibitor that could inhibit PI3Kα, PI3Kδ and PI3Kβ (31), was used in subsequent experiments. The results demonstrated that the combination of HpD-PDT and LY294002 showed a synergistic effect on the promotion of apoptosis, inhibition of cell viability and suppression of migration. The inhibitor of PI3K could enhance the curative effects of HpD-PDT. These findings could provide a novel clinical combination therapy that could be used for esophageal cancer treatment in the future.

The present study revealed that the ratios of p-PI3K/PI3K and p-mTOR/mTOR in the LY294002 + HpD-PDT group were significantly decreased compared with those in the HpD-PDT alone group (Fig. 5H). The LY294002 and control groups only exhibited statistical differences with regard to the ratio of p-mTOR/mTOR (Fig. 5H). The inconsistent protein expression levels suggested that the regulatory mechanism of HpD-PDT may not be limited solely to the PI3K/AKT/mTOR signaling pathway but may involve the regulation of multiple mechanisms.

In clinical practice, it has been observed that a significant proportion of patients with esophageal cancer undergoing first PDT treatment do not achieve optimal photodynamic results. A repeat endoscopy is necessary for these patients to receive the secondary PDT 24 h later (55,56). This phenomenon may be attributed to several factors, including large tumor volume, limited light penetration depth, variable responses to PSs and inter-patient variability. However, increasing light intensity, while more efficient in targeting the tumor, also carries the risk of inducing esophageal damage and substantial scarring, leading to esophageal stenosis, a condition particularly prevalent among patients with early esophageal cancer (50,55). Consequently, the pursuit of high-intensity light exposure in PDT comes with inherent risks.

Our primary objective was to enhance patient responsiveness to PDT, while minimizing its adverse effects. The potential of PI3K inhibitors to augment PDT efficacy offers the prospect of reducing intravenous PS dosages and light exposure intensities, thereby mitigating side effects and improving therapeutic outcomes.

The present experiments were exclusively conducted using the KYSE-150 poorly differentiated esophageal cancer cell line. To improve the generalizability of the present findings, a diverse array of cell lines should be used for validation. Furthermore, it is essential to establish animal tumor models to provide empirical validation for the present conclusions through *in vivo* experiments.

In conclusion, HpD-PDT could reduce esophageal cancer cell viability, induce apoptosis and inhibit migration by downregulating the PI3K/AKT/mTOR signaling pathway. The combination of HpD-PDT and an inhibitor of PI3K (LY294002) could enhance the therapeutic efficacy compared with that observed for HpD-PDT alone. Further investigations on combination therapy are required to achieve improved clinical outcomes.

Acknowledgements

Not applicable.

Funding

No funding was received.

Availability of data and materials

The datasets used and/or analyzed during the current study are available from the corresponding author on reasonable request.

Authors' contributions

XW, JN and XL conceived the study and conducted data analysis. XW and JN wrote the original draft, which was subsequently revised by LY and XL. XW and LY conducted the data interpretation. XW, JN, LY and XL confirm the authenticity of all the raw data.All authors read and approved the final manuscript.

Ethics approval and consent to participate

Not applicable.

Patient consent for publication

Not applicable.

Competing interests

The authors declare that they have no competing interests.

References

1. Sung H, Ferlay J, Siegel RL, Laversanne M, Soerjomataram I, Jemal A and Bray F: Global Cancer Statistics 2020: GLOBOCAN estimates of incidence and mortality worldwide for 36 cancers in 185 countries. CA Cancer J Clin 71: 209-249, 2021.
2. Morgan E, Soerjomataram I, Rumgay H, Coleman HG, Thrift AP, Vignat J, Laversanne M, Ferlay J and Arnold M: The global landscape of esophageal squamous cell carcinoma and esophageal adenocarcinoma incidence and mortality in 2020 and projections to 2040: New estimates from GLOBOCAN 2020. Gastroenterology 163: 649-658.e2, 2022.
3. Kato H and Nakajima M: Treatments for esophageal cancer: A review. Gen Thorac Cardiovasc Surg 61: 330-335, 2013.
4. Correia JH, Rodrigues JA, Pimenta S, Dong T and Yang Z: Photodynamic Therapy review: Principles, Photosensitizers, applications, and future directions. Pharmaceutics 13: 1332, 2021.
5. Dobson J, de Queiroz GF and Golding JP: Photodynamic therapy and diagnosis: Principles and comparative aspects. Vet J 233: 8-18, 2018.
6. Agostinis P, Berg K, Cengel KA, Foster TH, Girotti AW, Gollnick SO, Hahn SM, Hamblin MR, Juzeniene A, Kessel D, *et al*: Photodynamic therapy of cancer: An update. CA Cancer J Clin 61: 250-281, 2011.
7. Zahra M, Chota A, Abrahamse H and George BP: Efficacy of green synthesized nanoparticles in photodynamic therapy: A therapeutic approach. Int J Mol Sci 24: 10931, 2023.
8. Zhang X, Cai L, He J, Li X, Li L, Chen X and Lan P: Influence and mechanism of 5-aminolevulinic acid-photodynamic therapy on the metastasis of esophageal carcinoma. Photodiagnosis Photodyn Ther 20: 78-85, 2017.
9. Lan M, Zhao S, Liu W, Lee CS, Zhang W and Wang P: Photosensitizers for photodynamic therapy. Adv Healthc Mater 8: e1900132, 2019.
10. Kwiatkowski S, Knap B, Przystupski D, Saczko J, Kędzierska E, Knap-Czop K, Kotlińska J, Michel O, Kotowski K and Kulbacka J: Photodynamic therapy-mechanisms, photosensitizers and combinations. Biomed Pharmacother 106: 1098-1107, 2018.
11. van Gemert JC, Berenbaum MC and Gijsbers GH: Wavelength and light-dose dependence in tumour phototherapy with haematoporphyrin derivative. Br J Cancer 52: 43-49, 1985.
12. Kashyap D, Garg VK and Goel N: Intrinsic and extrinsic pathways of apoptosis: Role in cancer development and prognosis. Adv Protein Chem Struct Biol 125:73-120, 2021.
13. Carpenter R and Brady MF: BAX Gene. In: StatPearls [Internet]. Treasure Island (FL): StatPearls Publishing, 2023.
14. Cheung TH, Chung TK, Lo KW, Yu MY, Krajewski S, Reed JC and Wong YF: Apotosis-related proteins in cervical intraepithelial neoplasia and squamous cell carcinoma of the cervix. Gynecol Oncol 86: 14-18, 2002.
15. Korsmeyer SJ: BCL-2 gene family and the regulation of programmed cell death. Cancer Res 59 (7 Suppl): 1693s-1700s, 1999.
16. Thornberry NA and Lazebnik Y: Caspases: Enemies within. Science 281: 1312-1316, 1998.
17. Kumar D, Haldar S, Gorain M, Kumar S, Mulani FA, Yadav AS, Miele L, Thulasiram HV and Kundu GC: Epoxyazadiradione suppresses breast tumor growth through mitochondrial depolarization and caspase-dependent apoptosis by targeting PI3K/Akt pathway. BMC Cancer 18: 52, 2018.
18. Huang L, Lin H, Chen Q, Yu L and Bai D: MPPa-PDT suppresses breast tumor migration/invasion by inhibiting Akt-NF-κB-dependent MMP-9 expression via ROS. BMC Cancer 19: 1159, 2019.
19. Kumar S, Patil HS, Sharma P, Kumar D, Dasari S, Puranik VG, Thulasiram HV and Kundu GC: Andrographolide inhibits osteopontin expression and breast tumor growth through down regulation of PI3 kinase/Akt signaling pathway. Curr Mol Med 12: 952-966, 2012.
20. Liutkeviciute-Navickiene J, Mordas A, Rutkovskiene L and Bloznelyte-Plesniene L: Skin and mucosal fluorescence diagnosis with different light sources. Eur J Dermatol 19: 135-40, 2009.
21. Livak KJ and Schmittgen TD: Analysis of relative gene expression data using real-time quantitative PCR and the 2(-Delta Delta C(T)) Method 25: 402-408, 2001.
22. Gupta S, Dwarakanath BS, Muralidhar K and Jain V: Cellular uptake, localization and photodynamic effects of haematoporphyrin derivative in human glioma and squamous carcinoma cell lines. J Photochem Photobiol B 69: 107-120, 2003.
23. Pal M, Bhattacharya S, Kalyan G and Hazra S: Cadherin profiling for therapeutic interventions in Epithelial Mesenchymal Transition (EMT) and tumorigenesis. Exp Cell Res 368: 137-146, 2018.
24. Loh CY, Chai JY, Tang TF, Wong WF, Sethi G, Shanmugam MK, Chong PP and Looi CY: The E-Cadherin and N-Cadherin Switch in Epithelial-to-Mesenchymal Transition: Signaling, therapeutic implications, and challenges. Cells 8: 1118, 2019.
25. Glick D, Barth S and Macleod KF: Autophagy: Cellular and molecular mechanisms. J Pathol 221: 3-12, 2010.
26. Mizushima N and Komatsu M: Autophagy: Renovation of cells and tissues. Cell 147: 728-741, 2011.
27. Xie J, Wang S, Li Z, Ao C, Wang J, Wang L, Peng X and Zeng K: 5-aminolevulinic acid photodynamic therapy reduces HPV viral load via autophagy and apoptosis by modulating Ras/Raf/MEK/ERK and PI3K/AKT pathways in HeLa cells. J Photochem Photobiol B 194: 46-55, 2019.
28. Crowley LC and Waterhouse NJ: Detecting cleaved caspase-3 in apoptotic cells by flow cytometry. Cold Spring Harb Protoc 2016: 2016.
29. Li A, Qiu M, Zhou H, Wang T and Guo W: PTEN, insulin resistance and cancer. Curr Pharm Des 23: 3667-3676, 2017.
30. Chen CY, Chen J, He L and Stiles BL: PTEN: Tumor suppressor and metabolic regulator. Front Endocrinol (Lausanne) 9: 338, 2018.
31. Chaussade C, Rewcastle GW, Kendall JD, Denny WA, Cho K, Grønning LM, Chong ML, Anagnostou SH, Jackson SP, Daniele N and Shepherd PR: Evidence for functional redundancy of class IA PI3K isoforms in insulin signalling. Biochem J 404: 449-458, 2007.
32. Didamson OC and Abrahamse H: Targeted photodynamic diagnosis and therapy for esophageal cancer: Potential role of functionalized nanomedicine. Pharmaceutics 13: 1943, 2021.
33. Gallagher-Colombo SM, Finlay JC and Busch T: Tumor Microenvironment as a Determinant of Photodynamic Therapy Resistance. In: Resistance to Photodynamic Therapy in Cancer. Resistance to Targeted Anti-Cancer Therapeutics. Rapozzi V and Jori G (eds). Vol 5. Springer, Cham, pp65-97, 2015.
34. Rapozzi V and Jori G: Resistance to Photodynamic Therapy in Cancer. In: Resistance to Targeted Anti-Cancer Therapeutics. Vol 5. 1st edition. Springer, Cham, p248, 2015.
35. Rodrigues JA and Correia JH: Photodynamic therapy for colorectal cancer: An update and a look to the future. Int J Mol Sci 24: 12204, 2023.
36. Tahtamouni L, Ahram M, Koblinski J and Rolfo C: Molecular regulation of cancer cell migration, invasion, and metastasis. Anal Cell Pathol (Amst) 2019: 1356508, 2019.
37. Mao W, Sun Y, Zhang H, Cao L, Wang J and He P: A combined modality of carboplatin and photodynamic therapy suppresses epithelial-mesenchymal transition and matrix metalloproteinase-2 (MMP-2)/MMP-9 expression in HEp-2 human laryngeal cancer cells via ROS-mediated inhibition of MEK/ERK signalling pathway. Lasers Med Sci 31: 1697-1705, 2016.
38. Josefsen LB and Boyle RW: Unique diagnostic and therapeutic roles of porphyrins and phthalocyanines in photodynamic therapy, imaging and theranostics. Theranostics 2: 916-966, 2012.
39. Liu L, Ye Y and Zhu X: MMP-9 secreted by tumor associated macrophages promoted gastric cancer metastasis through a PI3K/AKT/Snail pathway. Biomed Pharmacother 117: 109096, 2019.
40. Jung JS, Jung K, Kim DH and Kim HS: Selective inhibition of MMP-9 gene expression by mangiferin in PMA-stimulated human astroglioma cells: Involvement of PI3K/Akt and MAPK signaling pathways. Pharmacol Res 66: 95-103, 2012.
41. Hwang YP, Yun HJ, Choi JH, Han EH, Kim HG, Song GY, Kwon KI, Jeong TC and Jeong HG: Suppression of EGF-induced tumor cell migration and matrix metalloproteinase-9 expression by capsaicin via the inhibition of EGFR-mediated FAK/Akt, PKC/Raf/ERK, p38 MAPK, and AP-1 signaling. Mol Nutr Food Res 55: 594-605, 2011.
42. Mathew R and White E: Autophagy in tumorigenesis and energy metabolism: Friend by day, foe by night. Curr Opin Genet Dev 21: 113-119, 2011.
43. He C, Xia J, Gao Y, Chen Z and Wan X: Chlorin A-mediated photodynamic therapy induced apoptosis in human cholangiocarcinoma cells via impaired autophagy flux. Am J Transl Res 12: 5080-5094, 2020.
44. Kma L and Baruah TJ: The interplay of ROS and the PI3K/Akt pathway in autophagy regulation. Biotechnol Appl Biochem 69: 248-264, 2022.

45. Xu Z, Han X, Ou D, Liu T, Li Z, Jiang G, Liu J and Zhang J: Targeting PI3K/AKT/mTOR-mediated autophagy for tumor therapy. Appl Microbiol Biotechnol 104: 575-587, 2020.
46. Heras-Sandoval D, Pérez-Rojas JM, Hernández-Damián J and Pedraza-Chaverri J: The role of PI3K/AKT/mTOR pathway in the modulation of autophagy and the clearance of protein aggregates in neurodegeneration. Cell Signal 26: 2694-2701, 2014.
47. Yan J, Dou X, Zhou J, Xiong Y, Mo L, Li L and Lei Y: Tubeimoside-I sensitizes colorectal cancer cells to chemotherapy by inducing ROS-mediated impaired autophagolysosomes accumulation. J Exp Clin Cancer Res 38: 353, 2019.
48. Fan TJ, Han LH, Cong RS and Liang J: Caspase family proteases and apoptosis. Acta Biochim Biophys Sin (Shanghai) 37: 719-727, 2005.
49. Elmore S: Apoptosis: A review of programmed cell death. Toxicol Pathol 35: 495-516, 2007.
50. Wang H, Ewetse MP, Ma C, Pu W, Xu B, He P, Wang Y, Zhu J and Chen H: The 'Light Knife' for gastric cancer: Photodynamic therapy. Pharmaceutics 15: 101, 2022.
51. Chen D, Wang B, Zhao Z, Zhang G, Wang P, Zhang L, Liu X, Zhang H, Zeng Q and Wang X: Modified 5-aminolevulinic acid photodynamic therapy induces cutaneous squamous cell carcinoma cell pyroptosis via the JNK signaling pathway. Biochim Biophys Acta Mol Cell Res 1871: 119603, 2023.
52. Li L, Song D, Qi L, Jiang M, Wu Y, Gan J, Cao K, Li Y, Bai Y and Zheng T: Photodynamic therapy induces human esophageal carcinoma cell pyroptosis by targeting the PKM2/caspase-8/caspase-3/GSDME axis. Cancer Lett 520: 143-159, 2021.
53. Pan WL, Tan Y, Meng W, Huang NH, Zhao YB, Yu ZQ, Huang Z, Zhang WH, Sun B and Chen JX: Microenvironment-driven sequential ferroptosis, photodynamic therapy, and chemotherapy for targeted breast cancer therapy by a cancer-cell-membrane-coated nanoscale metal-organic framework. Biomaterials 283: 121449, 2022.
54. Zhang ZJ, Huang YP, Li XX, Liu ZT, Liu K, Deng XF, Xiong L, Zou H and Wen Y: A Novel Ferroptosis-Related 4-Gene prognostic signature for cholangiocarcinoma and photodynamic therapy. Front Oncol 11: 747445, 2021.
55. Bartusik-Aebisher D, Osuchowski M, Adamczyk M, Stopa J, Cieślar G, Kawczyk-Krupka A and Aebisher D: Advancements in photodynamic therapy of esophageal cancer. Front Oncol 12: 1024576, 2022.
56. Yamashita H, Kadota T, Minamide T, Sunakawa H, Sato D, Takashima K, Nakajo K, Murano T, Shinmura K, Yoda Y, *et al*: Efficacy and safety of second photodynamic therapy for local failure after salvage photodynamic therapy for esophageal cancer. Dig Endosc 34: 488-496, 2022.